Available online at www.sciencedirect.com
SCIENCE DIRECT®
Journal of Structural Biology 143 (2003) 242–257
Journal of Structural Biology
www.elsevier.com/locate/yjsbi

Individual cartilage aggrecan macromolecules and their constituent glycosaminoglycans visualized via atomic force microscopy

Laurel Ng,[a] Alan J. Grodzinsky,[a,b,c] Parth Patwari,[b] John Sandy,[e] Anna Plaas,[f] and Christine Ortiz[d,*]

[a] *Biological Engineering Division, Massachusetts Institute of Technology, Cambridge, MA, USA*
[b] *Departments of Electrical Engineering and Computer Science, Massachusetts Institute of Technology, Cambridge, MA, USA*
[c] *Mechanical Engineering, Massachusetts Institute of Technology, Cambridge, MA, USA*
[d] *Materials Science and Engineering, Massachusetts Institute of Technology, Cambridge, MA, USA*
[e] *Department of Pharmacology and Therapeutics, College of Medicine, University of South Florida, Tampa, USA*
[f] *Department of Internal Medicine and Anatomy, College of Medicine, University of South Florida, USA*

Received 25 June 2003, and in revised form 7 August 2003

Abstract

Atomic force microscopy was used in ambient conditions to directly image dense and sparse monolayers of bovine fetal epiphyseal and mature nasal cartilage aggrecan macromolecules adsorbed on mica substrates. Distinct resolution of the non-glycosylated N-terminal region from the glycosaminoglycan (GAG) brush of individual aggrecan monomers was achieved, as well as nanometer-scale resolution of individual GAG chain conformation and spacing. Fetal aggrecan core protein trace length (398 ± 57 nm) and end-to-end length (257 ± 87 nm) were both larger than that of mature aggrecan (352 ± 88 and 226 ± 81 nm, respectively). Similarly, fetal aggrecan GAG chain trace length (41 ± 7 nm) and end-to-end (32 ± 8 nm) length were both larger than that of mature aggrecan GAG (32 ± 5 and 26 ± 7 nm, respectively). GAG–GAG spacing along the core protein was significantly smaller in fetal compared to mature aggrecan (3.2 ± 0.8 and 4.4 ± 1.2 nm, respectively). Together, these differences between the two aggrecan types were likely responsible for the greater persistence length of the fetal aggrecan (110 nm) compared to mature aggrecan (82 nm) calculated using the worm-like chain model. Measured dimensions and polymer statistical analyses were used in conjunction with the results of Western analyses, chromatographic, and carbohydrate electrophoresis measurements to better understand the dependence of aggrecan structure and properties on its constituent GAG chains.

Keywords: Cartilage; Aggrecan; Glycosaminoglycan; Chondroitin sulfate; Atomic force microscopy

1. Introduction

Aggrecan, the major load-bearing proteoglycan in the extracellular matrix of all cartilaginous tissues, is composed of a ~300 kDa core protein substituted with ~100 chondroitin sulfate (CS) and, in some species, keratan sulfate (KS) glycosaminoglycan (GAG) chains (Fig. 1A). Aggrecan is a member of the hyaluronan (HA)-binding proteoglycan family (which also includes brevican, neurocan, and versican) and associates noncovalently with HA and the ~45 kDa link glycoprotein to form high molecular weight aggregates (>200 MDa). In cartilage, these aggregates form a densely packed, hydrated gel that is enmeshed within a network of reinforcing collagen fibrils. Electrostatic repulsion forces between the highly negatively charged GAGs of aggrecan are known to provide >50% of the equilibrium compressive modulus of cartilage (Buschmann and Grodzinsky, 1995; Maroudas, 1979). Structural variations are known to exist as a function of age, disease, and species, including differences in GAG chain length, sulfate ester substitution, and KS and CS substitution (Plaas et al., 2001; Plaas et al., 1997). It is also known that progressive C-terminal truncation of the core protein by

* Corresponding author. Fax: 1-617-253-8779.
E-mail address: cortiz@mit.edu (C. Ortiz).

1047-8477/$ - see front matter © 2003 Elsevier Inc. All rights reserved.
doi:10.1016/j.jsb.2003.08.006

Abbreviations

AFM	atomic force microscopy
APTES	3-aminopropyltriethoxysilane
CS	chondroitin sulfate
DMMB	dimethyl methylene blue
EM	electron microscopy
FACE	fluorophore assisted carbohydrate gel electrophoresis
GAG	glycosaminoglycan
HA	hyaluronic acid
HRFS	high resolution force spectroscopy
IGD	interglobular domain
KS	keratan sulfate
NMR	nuclear magnetic resonance
QELS	quasielastic light scattering
SANS	small angle neutron scattering
SDS–PAGE	sodium dodecyl sulfate–polyacrylamide gel electrophoresis
TEM	transmission electron microscopy
TMAFM	tapping mode atomic force microscopy
WLC	worm-like chain
XPS	X-ray photoelectron spectroscopy
XRD	X-ray diffraction

proteolytic enzymes takes place with increasing maturation (Buckwalter et al., 1984; Buckwalter and Rosenberg, 1988; Dudhia et al., 1996; Flannery et al., 1992; Paulsson et al., 1987; Sandy and Verscharen, 2001).

Aggrecan, HA, and CS have been studied in solution by biophysical techniques such as small angle neutron scattering (SANS), quasielastic light scattering (QELS), X-ray diffraction (XRD), nuclear magnetic resonance (NMR), sedimentation, and viscosity (Cleland, 1977; Cleland and Wang, 1970; Hascall and Sajdera, 1970; Mathews and Decker, 1977; Perkins et al., 1981), as well as biochemical techniques such as electrophoresis and chromatography. This extensive body of literature is largely based on polydisperse populations of molecules,

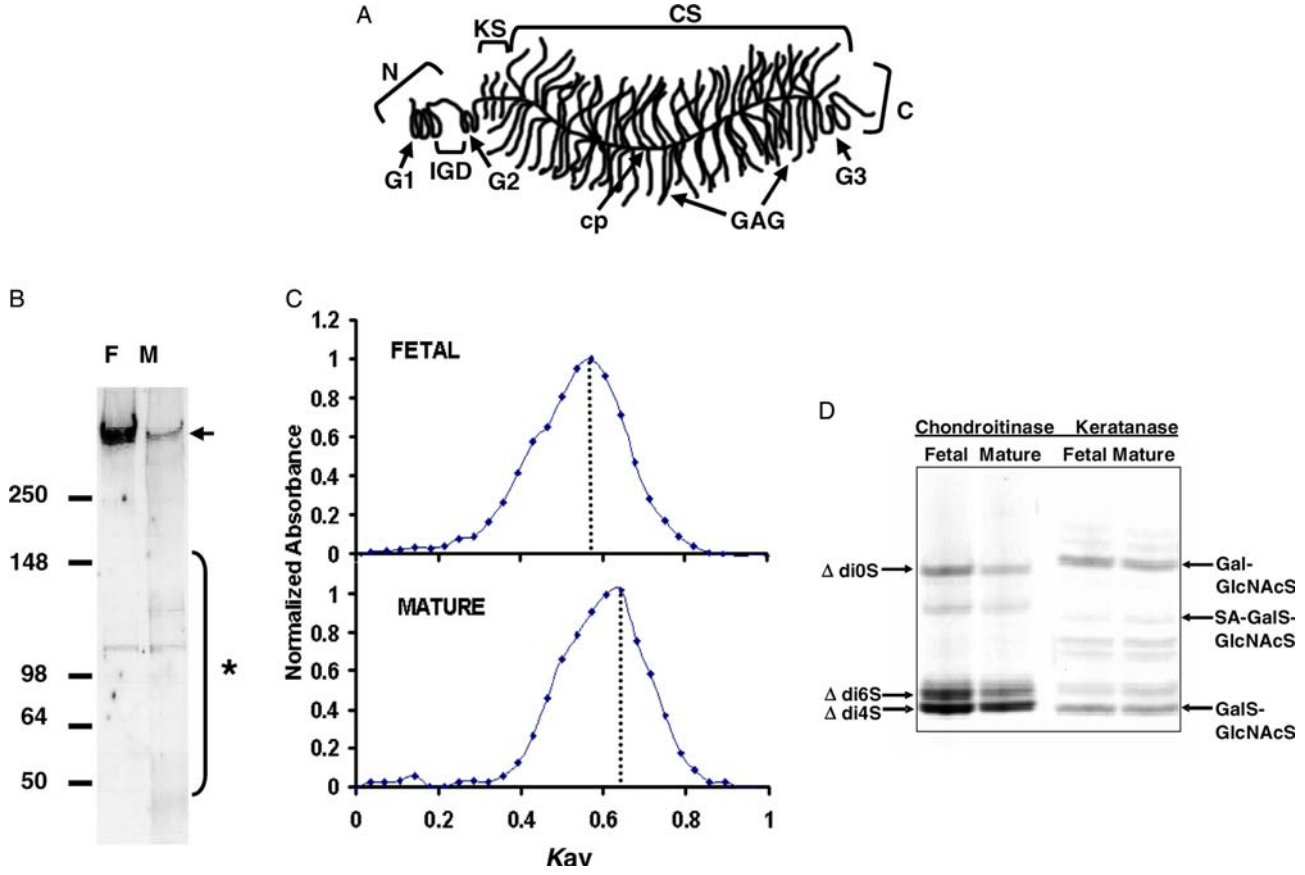

Fig. 1. (A) Structure of aggrecan: N, amine-terminal; G1, G2, G3, globular domains; IGD, interglobular domain between G1 and G2; cp, core protein; KS, keratan sulfate region; CS, chondroitin sulfate brush region; GAG, glycosaminoglycan chains; C, carboxyl-terminal. (B) Western blot analysis with anti-G1 peptide (JSCATEG) shows a high majority (>90%) of full-length core protein (arrow) with some evidence of a very small amount of C-terminally truncated core species (*) in the mature sample. (C) Superose 6 chromatograms show the fetal epiphyseal GAGs are longer than mature nasal GAGs with $K_{av} = 0.60$ and 0.64, respectively. (D) FACE gel of the fetal epiphyseal and mature nasal cartilage aggrecan GAG chains.

so the fine details of molecular heterogeneity, conformation, and structure at the level of the individual aggrecan molecule have not yet been obtained. Such molecular-level information is often crucial for theoretical models that are used to predict molecular interactions and macroscopic tissue behavior (Dean et al., 2003; Seog et al., 2002). Electron microscopy (EM) imaging has been used successfully to visualize fixed, dried, and metal-coated samples of cartilage proteoglycan aggregates as well as individual aggrecan monomers and reveal the presence of a thick CS-brush region and a thinner segment attached to HA (Buckwalter and Rosenberg, 1982; Morgelin et al., 1988; Rosenberg et al., 1970). While individual CS-GAG chains were occasionally resolved, they often appeared as collapsed bundles, making determination of their number, spacing, dimensions, and conformation difficult.

With the advent of high resolution atomic force microscopy (AFM), chemically and positionally sensitive force spectroscopy, nanoindentation, and the direct visualization and probing of numerous biological macromolecules (including DNA, proteins, and polysaccharides) in fluid and ambient conditions, nm-scale resolution has been achieved. Measurements have been made of the dimensions and conformation (e.g., persistence length and entanglements), supramolecular association, and nanomechanical properties of individual macromolecular chains in physiological and near-physiological conditions (Jarchow et al., 2000; Raspanti et al., 2001; Shao et al., 1996; Sheiko, 2000; Yamamoto et al., 1997). Researchers have recently begun to use these new nanotechnological tools in the study of cartilage and its constituent extracellular matrix (ECM) macromolecules. Fluid AFM and nanoindentation of articular cartilage sections, both native and after partial enzymatic digestion of the ECM proteoglycans, allowed for visualization and nanomechanical probing of the collagen fibril network (Cowman et al., 1998; Hunziker et al., 2002; Jurvelin et al., 1996). Individual bovine articular cartilage aggrecan forms were observed by AFM (Ng et al., 2002; Ng et al., 2003a), and reconstruction techniques that take into account the finite size and shape of the probe tip were employed to infer further structural information (Todd et al., 2003). Recently, we reported the distinct resolution of the N-terminal globular domains from the CS/KS-substituted "brush" region, as well as visualization of the individual CS-GAG chains of bovine cartilage aggrecan via AFM (Ng et al., 2003b). Here, we expand these initial studies and give a detailed quantitative comparison between bovine fetal epiphyseal and mature nasal cartilage aggrecan using a combination of biochemical, AFM, and polymer statistical methodologies. Our long term goal is to use these sample preparation, imaging, and data analysis techniques in conjunction with nanomechanical testing to gain insights into the function of cartilage ECM constituents.

2. Materials and methods

2.1. Purification of cartilage aggrecan

Mature nasal cartilage from 18-month-old bovines was removed, washed in ice-cold 50 mM sodium acetate, pH 7.0, containing a mixture of protease inhibitors, and stored on ice until further processing. The tissue was cut into $3 \times 3\,mm^2$ pieces and extracted in 4 M guanidium hydrochloride, 100 mM sodium acetate, pH 7.0, with protease inhibitors for 48 h. Unextracted tissue residues were separated by centrifugation and the clarified supernatant dialyzed against two changes of 100 volumes of 0.1 M sodium acetate, pH 7.0, with protease inhibitors (Buckwalter and Rosenberg, 1982; Hascall and Sajdera, 1969). Fetal bovine cartilage was obtained from the epiphyseal growth plate region, processed, and stored as described above. Purified aggrecan fractions (A1A1D1D1) were dialyzed consecutively against 500 volumes of 1 M NaCl and deionized water to remove excess salts. Aggrecan yield was determined by the dimethyl methylene blue (DMMB) dye-binding assay (Farndale et al., 1986).

2.2. Biochemical characterization of aggrecan and GAGs

Aggrecan preparations were analyzed for core protein heterogeneities by SDS–PAGE and Western blot analyses. Briefly, about 200 μg of fetal and 200 μg of mature aggrecan were digested at 37 °C with 30 mU chondroitinase ABC, 0.5 mU keratanase II, and 0.5 mU endobetagalactosidase. For Western analysis, 10% of each sample was lyophilized and then resuspended in a sample buffer of DTT (dithiothreitol), urea, and Tris–Gly SDS 2× sample buffer (BioRad Laemmli #161-0737). The sample was heat inactivated, loaded onto a 4–12% Tris–Gly gel, and the gel was run at 200 V for 40 min in an ice bath. Transfer to the blotting membrane was run at 100 V for 1 h and the membrane was blocked with TBS–T (Tris-buffered saline with Tween 20) with 1% dry nonfat milk for 10 min. The blots were probed with affinity-purified antibodies (Sandy and Verscharen, 2001) to either the aggrecan G1 domain (JSCATEG) or to the G3 domain (JSCTYK).

To determine the hydrodynamic radius of the CS-GAG chains, aggrecan preparations (200 μg as sulfated (S)-GAG) were first digested with 1.5 units/ml of papain in 0.1 M sodium acetate, pH 6.5. Desalting and separation of the CS from KS chains were done on a G50 sizing column. CS chains were liberated from the core protein by β-elimination in 100 mM sodium borohydride and 100 μM NaOH (Deutsch et al., 1995). Excess borohydride was reduced by addition of 50% acetic acid and samples rinsed with methanol. The dried samples were suspended in 0.5 M ammonium acetate, pH 7.3, assayed for CS content using DMMB, and

eluted on Superose 6 FPLC column (Amersham–Pharmacia Biotech) chromatography. Fractions (0.5 ml) were collected at 0.5 ml/min and assayed for S-GAG contents by DMMB and the average chain lengths of CS (number average disaccharides per chain) were computed from the K_{av} of the peak elution (Deutsch et al., 1995). GAG compositional analyses were performed by fluorophore assisted carbohydrate gel electrophoresis (FACE) using methods described in detail previously (Calabro et al., 2001; Plaas et al., 2001).

2.3. Sample preparation for AFM

Muscovite mica surfaces (SPI Supplies, West Chester, PA, #1804 V-5) were treated with 0.01% 3-aminopropyltriethoxysilane (APTES; Sigma Aldrich, St. Louis, MO) v/v MilliQ water (18 MΩ · cm resistivity, Purelab Plus UV/UF, US Filter, Lowell, MA). Sixty microliters of APTES solution was deposited onto freshly cleaved mica, incubated for 20–30 min at room temperature in a humidity controlled environment, rinsed gently with MilliQ water, and air dried. The silanol groups on the muscovite mica $[KAl_2[AlSi_3]O_{10}(OH)_2]$ were covalently bound to APTES via aminosilane chemistry to leave an amine group exposed on the mica surface (Fig. 2). The rms roughness of the APTES-mica was measured to be 9.9 Å by tapping mode AFM in air. X-ray photoelectron spectroscopy (XPS) was used to verify the amine-functionalization of the surface by comparison of the fluorine-to-nitrogen ratio after the surface amines were reacted with trifluoroacetic acid anhydride (Fig. 3). The aggrecan surface monolayer density was controlled via the solution concentration and incubation time. Dense monolayers were obtained by placing ~30 µl aliquots of aggrecan solution containing of 500 µg/ml GAG (measured from DMMB) on the surface for 30–40 min, while sparse monolayers of well-separated aggrecan monomers were obtain using ~60 µl aliquots of 250 µg/ml GAG incubated for 20–30 min. After incubation, the samples were gently rinsed in a stream of MilliQ water and air dried. Electrostatic interaction between the APTES-mica and the aggrecan GAG chains enabled retention of a population of aggrecan despite rinsing. Samples were imaged within a day of preparation.

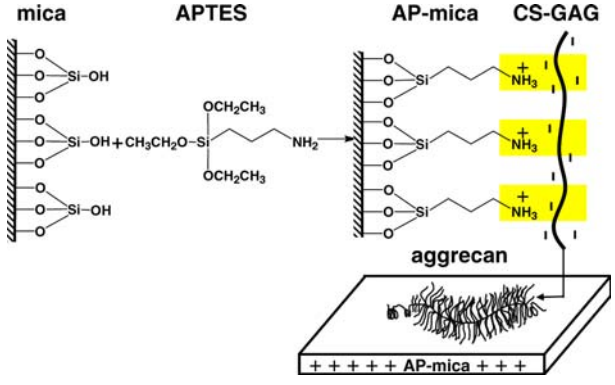

Fig. 2. AFM sample preparation. Silanol groups on the mica surface were functionalized with 3-aminopropyltriethoxysilane (APTES) producing surface amine groups ($pK_a = 10.5$) which were protonated in the neutral-buffered solution used for adsorption. This positively charged AP-mica surface facilitated electrostatic binding with the negatively charged COO^- and SO_3^- groups on the GAG chains to hold the aggrecan non-covalently on the surface.

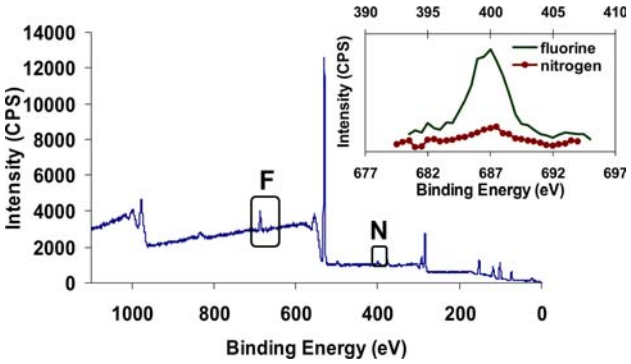

Fig. 3. Characterization of AP-mica. XPS data of the AP-mica surface show the presence of fluorine and nitrogen. The inset is a higher magnification of the nitrogen and fluorine peaks, which shows a 3:1 ratio of N:F confirming the presence of amine groups on the mica surface.

2.4. AFM imaging

The Nanoscope IIIa Multimode AFM (Digital Instruments (DI), Santa Barbara, CA) was used to image all samples via the EV or JV scanners. Tapping mode (TMAFM) was employed in ambient temperature and humidity using *Olympus* AC240TS-2 rectangular Si cantilevers ($k = 2$ N/m). Scanning electron microscopy (SEM, JOEL 6320FV) was employed to characterize the probe tip (Fig. 4) and typical end-radii were found to be

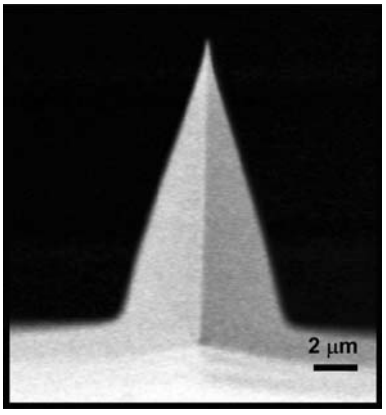

Fig. 4. SEM of tapping mode probe tip for AFM imaging.

<10 nm. The cantilever was driven just below resonant frequency, ω_0, and a slow scan rate of 1–3 Hz was used to minimize sample disturbances giving a scan rate that was much slower (<25 000×) than the tap rate. The maximum sample size of 512×512 pixels was used. The system was allowed to pre-equilibrate for at least 30 min. prior to imaging to minimize drift. The drive amplitude and amplitude set-point were maximized to get the fullest peak upon tuning. Gains were chosen to maximize either the height image (gains ~0.65) or the amplitude image (gains ~0.1). The rms amplitude (~27 nm) of the cantilever oscillation at resonant frequency was determined by increasing the Z scan start and plotting the amplitude versus z-position on the force calibration plot in tapping mode. At these z-amplitudes, attractive forces due to any water meniscus capillarity are overcome (Tamayo and Garcia, 1996). The x- and y-scan directions were calibrated with a $10 \times 10\,\mu m^2$ grid. The z-direction was calibrated with 5 nm diameter gold particles (Ted Pella Inc.) on a cleaved mica surface. The scans were tested for typical AFM imaging artifacts by varying scan direction, scan size, and rotating the sample.

2.5. Calculation of trace, end-to-end, and effective persistence lengths from AFM images

Using SigmaScan Pro image analysis software (SPSS Science, Chicago, IL), the core protein and GAG contour lines in the AFM images were digitized into pixels yielding the spatial coordinates of each position along the polymer chain. The trace lengths, L_c, and end-to-end lengths, R_{ee}, were measured directly from these images. For reference, μ represents the mean, n represents the number of data points, and $\pm$ symbolizes one standard deviation. An effective persistence length, L_p, a parameter related to the local chain stiffness of the core protein as well as the individual GAGs, was also calculated assuming the validity of the Kratky–Porod Worm-Like Chain (WLC) model (Kratky and Porod, 1949)) which describes a polymer chain that is intermediate between a rigid-rod and a flexible coil and takes into account both local stiffness as well as long-range flexibility. The WLC model represents an isolated polymer chain as an isotropic, homogeneous elastic rod whose trajectory varies continuously and smoothly through space. The chain consists of n rotating unit vectors (statistical segments) of length l joined in succession, where each vector is oriented at an angle θ with respect to the previous vector (shown Section 3). For 2D conformations obtained after surface equilibration (as opposed to "kinetic trapping") (Rivetti et al., 1996), the probability density $P(\theta(l))$ of the bend angle $\theta(l)$ is theoretically expected to be normally distributed with mean zero and variance, $\langle\theta^2(l)\rangle$, as shown below:

$$P(\theta(l))_{2D} = \sqrt{\frac{L_p}{2\pi l}} \exp\left(-\frac{L_p \theta(l)^2}{2l}\right), \tag{1}$$

$$\langle\theta^2(l)\rangle = \left(\frac{l}{L_p}\right). \tag{2}$$

To verify that the observed values of $\theta(l)$ were consistent with the behavior predicted by the WLC model and that the 2D images were equilibrated on the surface (i.e., representative of the 3D conformation), the normality of θ was assessed at different levels of l by examination of the distribution of θ on histograms and by calculation of kurtosis

$$\text{kurtosis} = \frac{\langle\theta^4(l)\rangle}{\langle\theta^2(l)\rangle^2} - 3. \tag{3}$$

Kurtosis, defined by Eq. (3), is an indication of the peakedness of the distribution (i.e., whether the shape of the distribution is more or less peaked compared to the normal distribution), and equals zero for a normally distributed variable. It has previously been interpreted as an assessment of the observed 2D conformations (Rivetti et al., 1996; Round et al., 2002).

To obtain θ as a function of l from the images, a series of equal length vectors was iteratively projected onto the digitized trace of the core protein and GAG contours from $5l$ ($l \sim 1.2$ nm) to xl ($x = 35$, $xl \sim 42$ nm) in increments of l. The angle θ between consecutive vectors was calculated over the length of the molecule. The linear relationship of the variance of θ as a function of l was then used to estimate an effective persistence length L_p for aggrecan molecules and for GAG chains. For each image of a molecule, the variance of θ was estimated at multiple values of l. These resulting estimates of variance are thus not independent but correlated with the molecule image from which they were obtained. A linear mixed-effects analysis (Diggle et al., 1994) was performed (SPlus, MathSoft; now Insightful, Seattle, WA). Molecule-to-molecule variation was included as a random effect in the model and l was included as a fixed effect. In addition, an indicator variable, z, was used to identify whether the aggrecan was from mature ($z = 1$) or fetal ($z = 0$) cartilage. To test for differences between L_p from mature and fetal aggrecan, the statistical significance of the interaction term between z and l was assessed, since this term represents the difference in the slopes of the lines relating the variance of θ to l. The full model for the fixed effects was thus

$$s^2(\theta) = \beta_0 + \beta_1 \cdot l + \beta_2 \cdot z + \beta_3 \cdot l \cdot z, \tag{4}$$

where s^2 is the sample variance and β_i is the estimated coefficients. L_p was calculated as the inverse of β_1, since this coefficient is equal to $1/L_p$ for the WLC, as described above. An equivalent model was used to estimate L_p for GAG chains and to test for differences between L_p of fetal and mature GAG.

3. Results

3.1. Biochemical characterization of aggrecan and GAGs

Western analysis with antibody JSCATEG specific to the G1 domain (Fig. 1B) suggested that the majority of aggrecan core protein species (>90%) in these samples were high molecular weight (~350 kDa) full-length molecules for both the fetal and mature preparations. Identification of the single major band in each preparation as the full-length species was confirmed by showing immunoreactivity of this band with antibody JSCTYK which reacts with an epitope at the extreme C-terminus of the G3 domain (data not shown). While the predominant aggrecan core species detected (>90%) was full length, there was evidence of C-terminally truncated species of very low abundance (Fig. 1B). The average chain length of GAGs from fetal epiphyseal aggrecan was calculated from Superose 6 chromatograms (Fig. 1C) to be ~50 disaccharides (corresponding to ~48 nm), while that from nasal aggrecan was ~42 disaccharides (corresponding to ~40 nm). FACE gel analyses of aggrecan GAG chains (Fig. 1D) revealed that the fetal epiphyseal GAG had a CS:KS ratio three times higher than that of the mature nasal GAG. The chondroitin-4-sulfate disaccharide (C4S) amount was higher than the chondroitin-6-sulfate (C6S) for the mature aggrecan, whereas the C4S and C6S contents were essentially equal in the fetal aggrecan (Fig. 1D, Table 1).

3.2. Visualization of dense and sparse aggrecan monolayers

Tapping mode AFM images of dense monolayers of fetal epiphyseal aggrecan showed that individual aggrecan monomers (Fig. 5A) and their constituent GAG chains (Fig. 5B) are clearly resolved. The monomers exhibited varying degrees of extension and did not appear to be aligned in any preferred direction. Rather, they conformed to each other to create a dense packing on the 2D surface suggesting that the core protein backbone had some degree of flexibility. At higher magnification (Fig. 5B, boxed regions), interdigitation between GAG chains of adjacent aggrecan molecules could sometimes be observed. More structural details of individual aggrecan molecules became apparent on lower density monolayers (representative images, Fig. 6) where the thicker GAG brush region can be clearly distinguished from the thinner N-terminal region. As observed in dense monolayers, the monomers in sparse monolayers exhibited varying degrees of extension and, again, were not aligned in any preferred direction. The heights of the aggrecan monomers were found to be approximately equal to the diameter of one GAG chain (~1 nm, Tanaka, 1978) suggesting that the aggrecan molecules appeared fully flattened on the surface, possibly due to surface attractive interactions and/or compression by the tip during imaging. "Thinner" aggrecan monomers (marked ** in Fig. 6A) were occasionally apparent and were found to have heights of ~2 GAG chains; hence, the GAG chains of such monomers were likely collapsed or folded over, and were not necessarily shorter than those of the much more numerous fully flattened aggrecan. The widths of the CS-GAG brush region, a reflection of GAG extension, were found to exhibit a continuous distribution with 57 ± 11 nm for the fetal and 47 ± 12 nm for the mature. Compared to fetal aggrecan (Fig. 6A), the size and structure of mature aggrecan (Fig. 6B) appeared more dimensionally heterogeneous, as manifest in the distributions of the aggrecan and GAG contour and end-to-end lengths (Table 2).

A side-by-side comparison of higher resolution images of individual (fully flattened) fetal epiphyseal versus mature nasal aggrecan (Fig. 7A) revealed the detailed nanoscale differences between these two populations with marked clarity. Close examination of the N-terminal region showed no distinct GAG attachment in this part of the core protein (Fig. 7B). The globular domains, G1 and G2, could not be easily resolved as these domains may have collapsed since the 135 amino acid sequence joining them forms a flexible chain (Hering et al., 1997). The trace length of the core protein component of the molecules in Fig. 7A were measured, 470 nm (fetal) and 396 nm (mature), and the widths of the brush-like GAG region were 96 nm (fetal) and 65 nm (mature). In addition, the GAG chains on the fetal monomer appeared longer and more extended. It was more difficult to distinguish individual CS-GAG chains in the brush region of mature aggrecan (e.g., Fig. 7C).

Table 1
Results on GAG chains from size exclusion chromatography (first column), DMMB assay (second column), and FACE (remaining columns). Below, S denotes sulfated

		# Disacch.	μg	0 sulfation	6 sulfated	4 sulfated	% monoS	% diS
Fetal	CS	50	13.1	10.5	38.3	51.2	—	—
	KS	—	0.33	—	—	—	38	62
Mature	CS	42	12.1	5.5	65.6	28.9	—	—
	KS	—	0.95	—	—	—	42	58

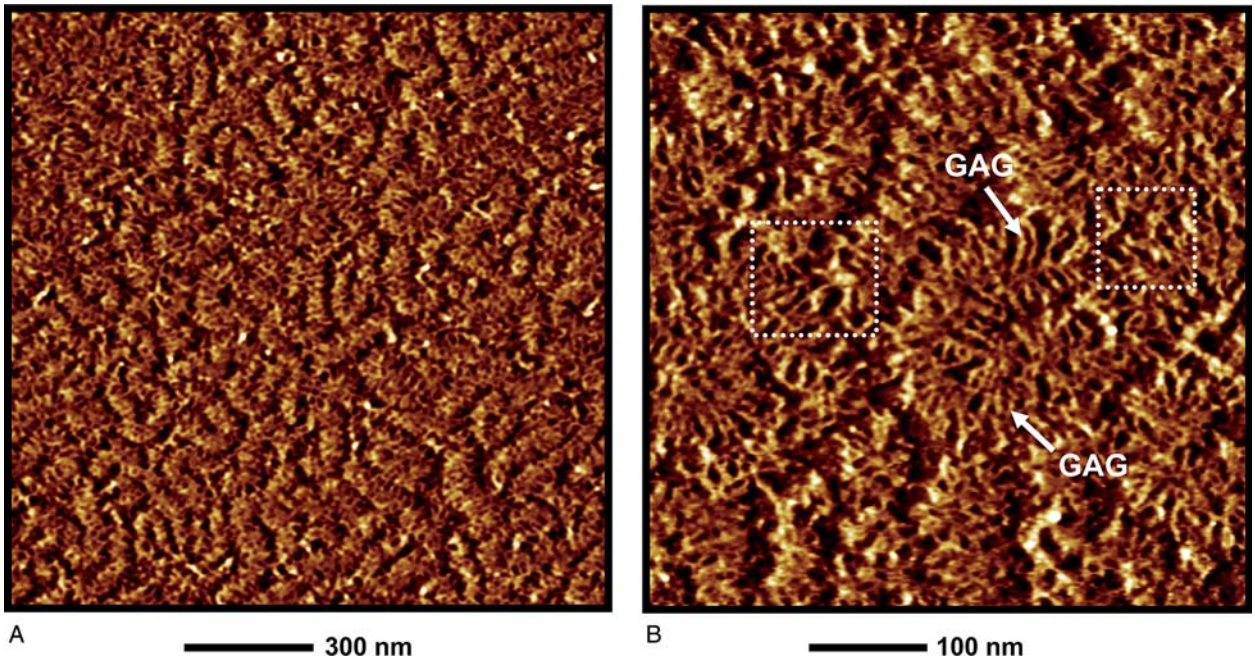

Fig. 5. Amplitude AFM images of fetal epiphyseal aggrecan monomers in (A) a dense monolayer. (B) Center region of (A) magnified. Boxed regions indicate interdigitation of GAG chains. The height is read with the darkest color as the baseline.

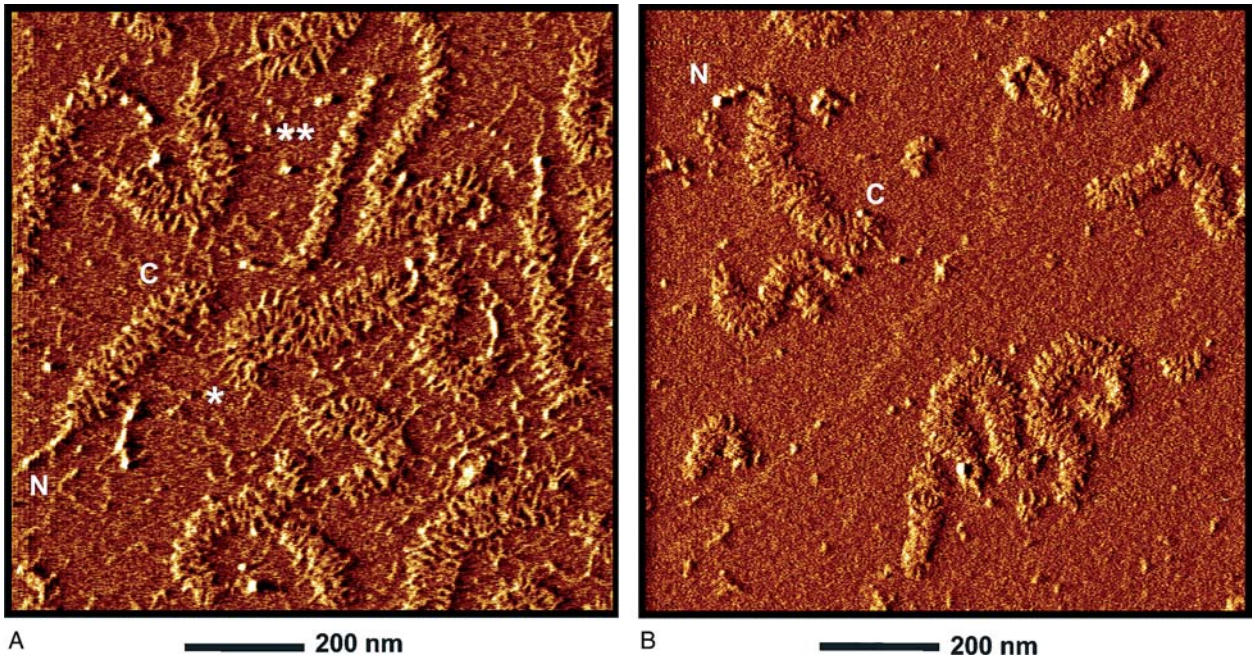

Fig. 6. Amplitude AFM images of lower density monolayers of (A) fetal epiphyseal and (B) mature nasal aggrecan. N- and C-terminal regions of the aggrecan are denoted on the images. GAG chains take on an extended (*) form, or occasionally a collapsed (**) form.

This may be attributed to the higher density of keratan sulfate relative to chondroitin sulfate chains along the core protein of mature aggrecan and/or other structural differences. To measure the distance between GAG chains in the brush region, cross-sections of the images were taken near the point of GAG attachment to the core protein (Fig. 8). The distribution of GAG spacing for the fetal and mature monomers of Fig. 8A is shown in the frequency histograms of Fig. 8C and the mean distance between GAG chains was found to be 3.2 ± 0.8 nm for the fetal aggrecan and 4.4 ± 1.2 nm for the mature aggrecan monomers.

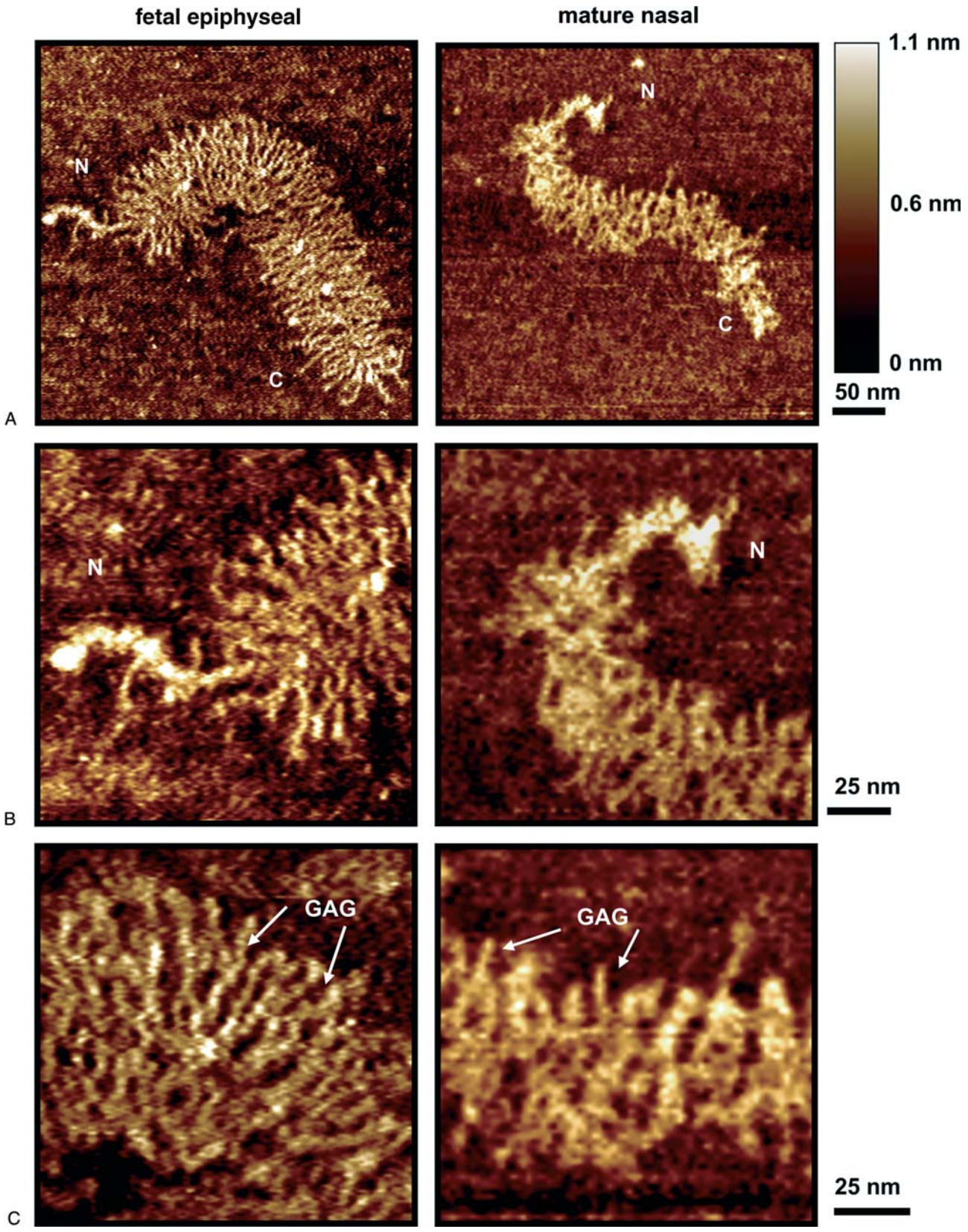

Fig. 7. Higher resolution comparison of AFM height images of an individual isolated: (A) fetal epiphyseal and mature nasal aggrecan monomer; (B) core protein visible in the N-terminal region on both monomers; (C) GAG chains, clearly visible in the CS-brush region, on both the mature and fetal monomers appear shorter on the mature nasal versus fetal epiphyseal.

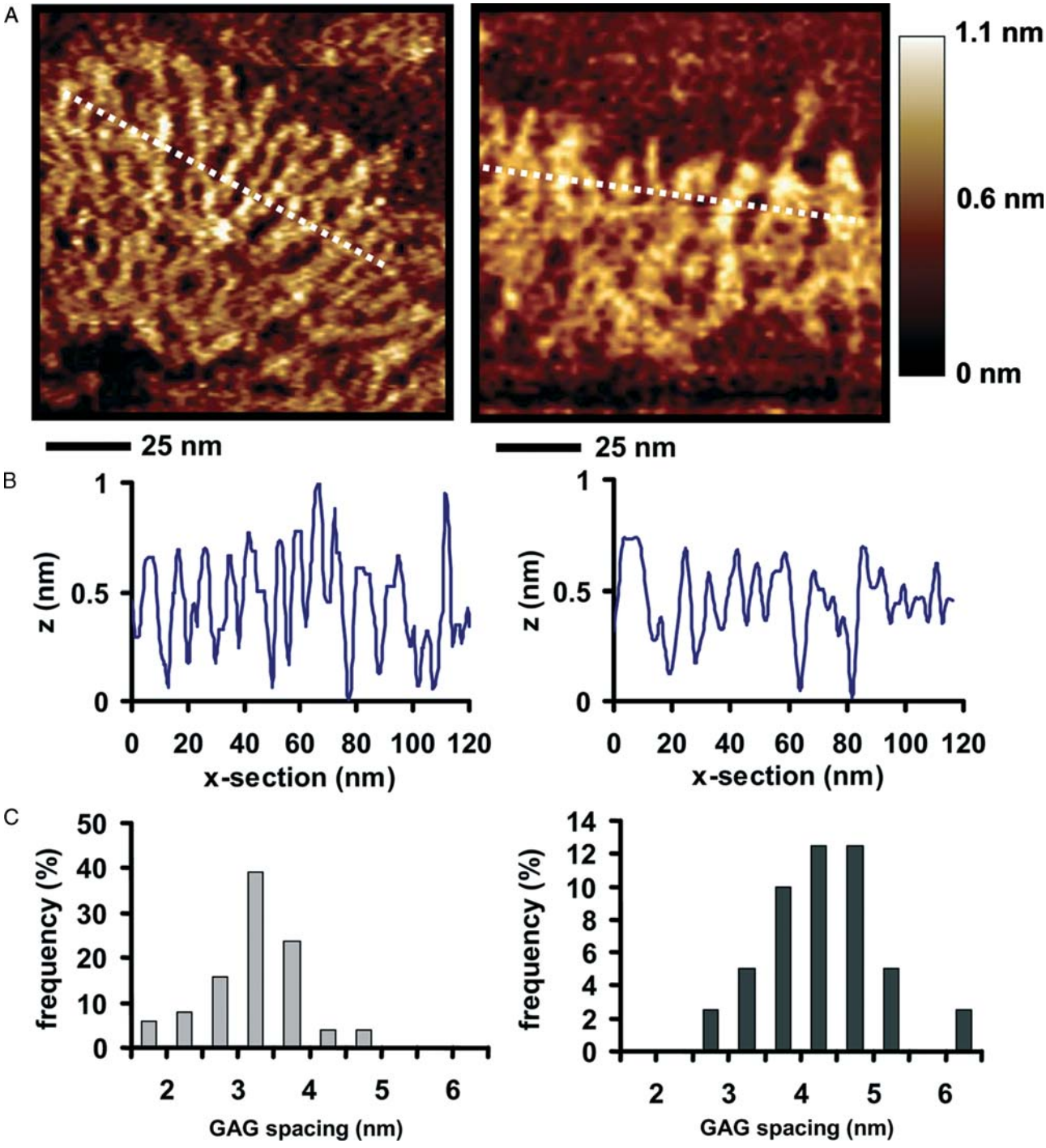

Fig. 8. (A) Higher resolution comparison of AFM height images of the fetal epiphyseal (left) and the mature nasal (right) aggrecan CS-brush region. (B) Cross-sectional profiles of the GAG spacing along one side of the core protein, corresponding to the white dotted lines of (A). (C) Histograms of GAG spacing between chains of fetal epiphyseal ($\mu = 3.2 \pm 0.8$ nm; $n = 102$) and mature nasal ($\mu = 4.4 \pm 1.2$ nm; $n = 40$).

3.3. Statistical analysis of trace and end-to-end lengths of core protein and CS-GAG chains

The trace of the core protein of individual aggrecan monomers from multiple images was digitized into pixels yielding the spatial coordinates of each position along the polymer chain. The trace lengths, L_c, and end-to-end lengths, R_{ee}, shown in Fig. 9A, were measured directly from these images and the probability distribution histograms calculated (Fig. 9B and C, Table 2). L_c was found to be 398 ± 57 nm for fetal compared to 352 ± 88 nm for mature, and R_{ee} was 257 ± 87 nm for

Table 2
Summary of measured dimensions from AFM images of aggrecan

	$L_{c,total}$ (nm)	R_{ee} (nm)	GAG spacing (nm)	$L_{c,barecoreprotein}$ (nm)	$L_{c,CS-brush}$ (nm)
Mature nasal aggrecan	352 ± 88 ($n = 141$)	226 ± 81 ($n = 141$)	—	81 ± 17 ($n = 29$)	268 ± 73 ($n = 29$)
Fetal epiphyseal aggrecan	398 ± 57 ($n = 113$)	257 ± 87 ($n = 113$)	—	93 ± 14 ($n = 29$)	327 ± 43 ($n = 29$)
Mature nasal GAG	32 ± 5 ($n = 49$)	26 ± 7 ($n = 49$)	4.4 ± 1.2 ($n = 40$)	—	—
Fetal epiphyseal GAG	41 ± 7 ($n = 102$)	32 ± 8 ($n = 102$)	3.2 ± 0.8 ($n = 102$)	—	—

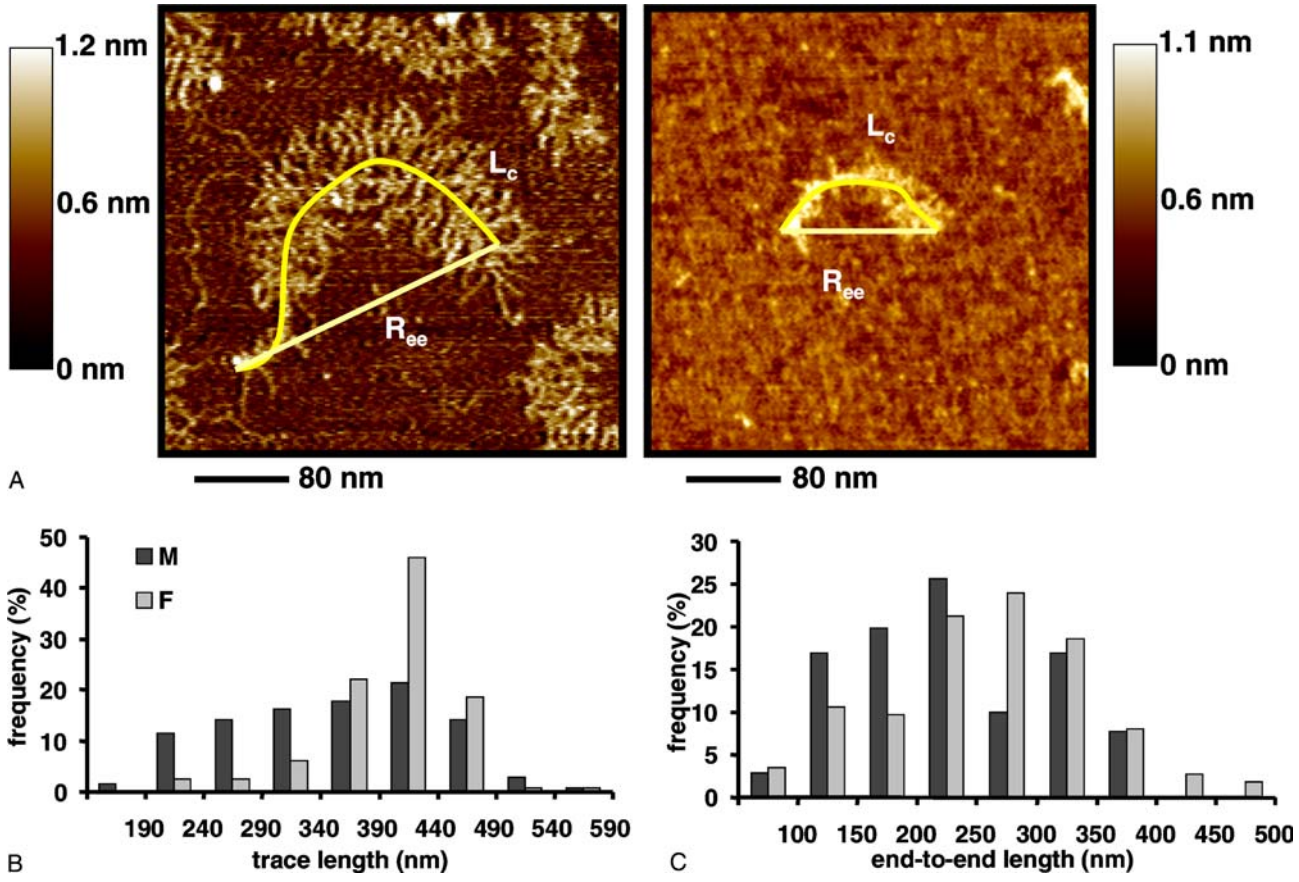

Fig. 9. (A) AFM height image in air of an individual isolated fetal epiphyseal aggrecan monomer (left) and a mature nasal aggrecan monomer (right). A trace of the aggrecan contour core protein is indicated by L_c and the end-to-end distance measurement is indicated by R_{ee}. (B) The histogram of aggrecan L_c shows that mature nasal aggrecan (M) ($L_c = 352 \pm 88$ nm; $n = 141$) is slightly shorter and has a broader distribution than the fetal epiphyseal aggrecan (F) ($L_c = 398 \pm 57$ nm; $n = 113$). (C) The histogram of R_{ee} for mature nasal aggrecan ($R_{ee} = 226 \pm 81$ nm) and fetal epiphyseal aggrecan ($R_{ee} = 257 \pm 87$) follow the same trend.

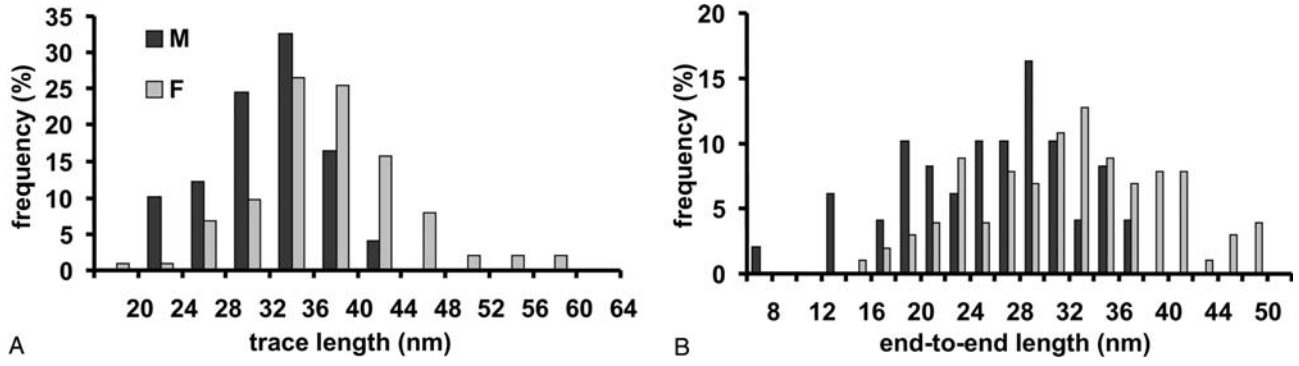

Fig. 10. Histograms show that the contour trace length L_c (left) of mature nasal GAG (M) ($\mu = 32 \pm 5$ nm; $n = 49$) was shorter than L_c of fetal epiphyseal GAG (F) ($\mu = 41 \pm 7$ nm; $n = 102$). The R_{ee} (right) of mature nasal GAG ($\mu = 26 \pm 7$ nm) was shorter than that of fetal epiphyseal GAG ($\mu = 32 \pm 8$ nm).

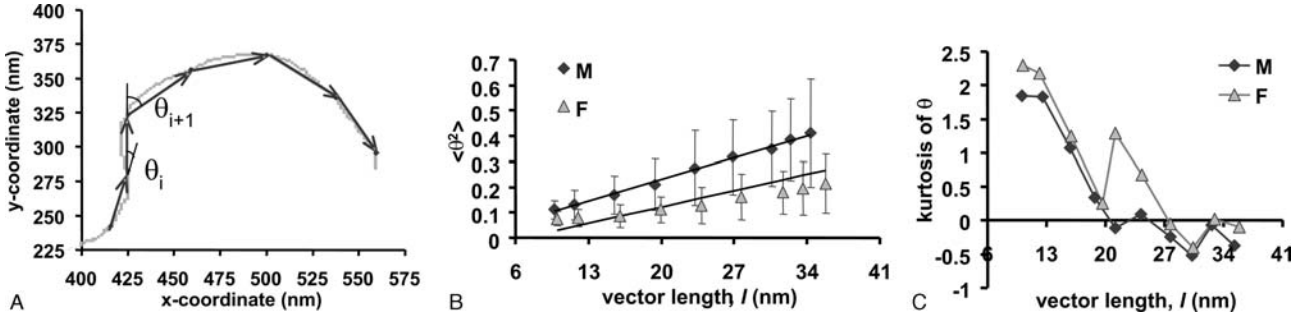

Fig. 11. (A) Trace for a single fetal epiphyseal aggrecan monomer (see Fig. 9A) from an AFM image. Vectors of length, l, were projected onto the trace. An angle was calculated from consecutive vectors and used in the calculation of persistence length. (B) $\langle\theta^2\rangle$ versus vector length l (nm) comparing mature nasal (M) ($n = 15$) and fetal epiphyseal (F) ($n = 15$) aggrecan monomers measured from AFM images. L_p, mature = 82 nm; L_p, fetal = 110 nm (see 95% confidence intervals in Table 3). (C) Kurtosis of θ versus l (nm) was plotted for the same population of monomers examined in (B) to determine if the Gaussian distribution of angles was maintained from the 3D to the 2D state.

Table 3
Persistence length calculated from AFM images of individual aggrecan monomers using the mixed effects statistical model

	Mature nasal aggrecan	Fetal epiphyseal aggrecan	Mature nasal GAG	Fetal epiphyseal GAG
L_p (nm), mean	82	110	14	21
95% Confidence interval (nm)	73–94	102–120	10–21	17–25

fetal compared to 226 ± 81 nm for mature aggrecan. The average extension of the core protein, defined as (R_{ee}/L_c), was 65 and 64% for fetal and mature, respectively. More than 75% of the extension distribution was clustered between 50 and 95% for nasal and 50 and 90% for epiphyseal (data not shown).

L_c and R_{ee} for the GAG chains (Fig. 10) were found to be 32 ± 5 and 26 ± 7 nm for the mature nasal versus 41 ± 7 and 32 ± 8 nm for the fetal epiphyseal, yielding an average GAG chain extension of 80 and 78% for mature nasal and fetal epiphyseal, respectively. More than 75% of the extension distribution was clustered between 70 and 95% for both mature nasal and fetal epiphyseal GAGs, respectively (data not shown). For the molecules in which the CS-brush region was well defined and distinguishable from the N-terminal bare core protein region, the contour length of each of these regions was measured separately. L_c of the bare N-terminal region was found to be 93 ± 14 and 81 ± 17 nm for fetal and mature aggrecan, respectively. A greater difference in L_c was found for the CS-brush region, 327 ± 43 and 268 ± 73 nm, for the fetal and mature, respectively (Table 2).

3.4. Persistence length measurements of core protein and GAG chain

In the calculation of the aggrecan core protein persistence length, the values for the vector segment lengths l were limited on the lower bound by pixelation of the trace and limited on the upper bound at $l < L_c$ (Fig. 11A). Statistical analysis of the linear relationship between $\langle\theta^2\rangle$ and l resulted in an effective mean core protein L_p of 110 nm for whole fetal epiphyseal aggrecan and 82 nm for whole mature nasal aggrecan (Fig. 11B, Table 3). This difference was found to be statistically significant (see 95% confidence intervals in Table 3). The mean effective L_p values for fetal epiphyseal and mature nasal GAG were 21 and 14 nm, respectively, but were not significantly different. The degree to which the observed 2D angles reflected the behavior predicted by the WLC model was assessed by calculation of the kurtosis of θ versus l (Fig. 11C). At larger values of l, the kurtosis was nearly zero for both aggrecan and GAG chains, as predicted for a normally distributed variable. A distribution plot of θ showed deviation from the Gaussian distribution at $\theta = \pi/4$ and $\pi/2$ for the lower values of l, suggesting that this deviation is probably due in part to the effects of pixelation.

4. Discussion

In this study, we first presented methodologies for the direct high resolution visualization of individual aggrecan monomers using the technique of tapping mode AFM. We then quantitatively assessed the contour, end-to-end, and persistence lengths of fetal epiphyseal aggrecan monomers and contrasted these parameters with those of mature nasal monomers.

4.1. General methodology for high resolution AFM imaging of aggrecan

High purity aggrecan (A1A1D1D1) was used to minimize nonspecific adsorption of other biomolecules onto the APTES-mica surface which could obscure the resolution of the target macromolecule (aggrecan)

during imaging. Minimal sample preparation was employed (no fixation, coating, or other chemical treatments). The negatively charged GAGs facilitated electrostatic binding of aggrecan to the APTES-mica amine groups ($pK_a \sim 10.5$). Since a thin layer of water ($\sim$2–10 Å thick) exists on the mica surface (Sheiko and Moller, 2001) even in ambient conditions, electrostatic-binding interactions are maintained and minimize lateral displacements of the aggrecan during imaging. This adsorbed water layer partially binds to and hydrates the hydrophilic aggrecan and its GAGs, helping to preserve near physiological conditions. Tapping mode in air was found to produce the highest resolution using relatively soft cantilevers and low set points to minimize sample deformation, damage, and displacement due to the forces exerted by the probe tip during imaging. Even though the probe tip end-radii were up to 10 nm or greater, resolutions down to or below 1 nm were achieved presumably due to an individual asperity or smaller region of the probe tip forming the actual contact during imaging (Shao et al., 1996). In many cases, however, "tip broadening" artifacts are frequently reported in the literature (Todd et al., 2003), where the biomolecular dimensions at high resolutions are overestimated due to the finite size and shape of the probe tip.

4.2. Comparison of aggrecan core protein dimensions and conformation assessed by AFM, EM, and biochemical methods

One major result of these AFM studies was the fact that the mature nasal aggrecan showed a slightly broader distribution of L_c shifted to lower values compared to the fetal epiphyseal aggrecan. Previous EM studies (Buckwalter and Rosenberg, 1982, 1983, 1988; Rosenberg et al., 1970) on bovine mature nasal and fetal epiphyseal aggrecan and their self-assembled aggregates (aggrecan non-covalently bound to HA) have reported dimensions such as trace length L_c of core protein, GAG chains, and HA, as well as the number of attached aggrecan to HA. While the differences in EM versus AFM sample preparation techniques make it difficult to compare absolute values of L_c obtained by these two techniques, the same trend of relative reduction in L_c of the core protein with age was observed by EM, though higher values of L_c were found by AFM (by as as much as 10–40%). The L_c of the G1–IGD–G2 core protein regions measured by AFM was slightly shorter than EM measurements.

Western analysis (Fig. 1B) suggested that the large majority of the high buoyant density preparations from both fetal and mature cartilages used in this study were full-length aggrecan, and since C-terminal truncation of the core protein by proteases appears to occur in distinct regions to generate discrete products of defined size ranges (Sandy and Verscharen, 2001), it is unlikely that there is an abundance of such high molecular weight truncated species present in these samples. If the distribution of surface adsorbed aggrecan measured by AFM is similar to the distribution of aggrecan in the starting solution (i.e., containing predominantly full-length core protein), then the distribution of core protein trace lengths measured by AFM (Fig. 9B) can be interpreted as that associated with full-length core protein extended to various degrees. Conformational and secondary structure variations of the core protein in the CS-brush region will most likely be affected by repulsive intra- and intermolecular GAG–GAG electrostatic double layer interactions, the range of which is determined by the GAG length, spacing, and heterogeneity. The observed reduction in the trace length for the mature sample compared to the fetal could arise from a number of different sources including: (1) entropic collapse to a more random coil-like configuration, (2) formation of additional intramolecular noncovalent bonds (e.g., "protein folding"), or (3) enthalpic changes due to a reduction in the individual amino acid bond angles. This interpretation is consistent with EM studies (Morgelin et al., 1989) which reported aggrecan core protein trace lengths that were significantly shorter in the deglycosylated form (263 ± 27 nm) compared to the glycosylated form (405 ± 37 nm).

It should be noted that the distribution of surface adsorbed aggrecan does not necessarily have to be equivalent to the distribution of aggrecan in the starting solution and, hence, there does exist the possibility that the shorter length monomers observed by AFM could in part be C-terminally truncated aggrecan monomers (Sandy and Verscharen, 2001) that preferentially adsorbed to the surface. However, in the absence of transport limitations, preferential adsorption of smaller molecules is unlikely since larger molecules have a greater number of attractive contacts holding them down as well as a greater attractive interaction force on approach to the surface.

Even though statistically significant differences in the trace contour lengths and end-to-end lengths were observed for the two aggrecan populations, it is interesting to note that the average larger length scale extension ratios (R_{ee}/L_c) (Fig. 9) were essentially the same. If the molecules have conformations that have equilibrated in 2D on the surface, the fact that R_{ee}/L_c (Fig. 9) for both the mature and fetal aggrecan populations were found to be essentially the same suggests that the molecular origin of these parameters, presumably GAG–GAG electrostatic double repulsion, is the same. R_{ee} clearly represents straightening or bending of the whole aggrecan molecule as directly visualized by the AFM images and we have suggested that the trace length, L_c, reflects the extension or compression along the main core protein backbone. Both of these parameters reflect an equilibrium balance

between repulsive (e.g., electrostatic double layer forces imparted by CS-GAGs and determined by CS-GAG length, spacing, etc.) and attractive (e.g. entropic, non-covalent bonding) intra- and intermolecular interactions.

4.3. Comparison of CS-GAG dimensions and conformation assessed by AFM and biochemical methods

Another major result of this AFM study was the fact that for the first time, unmodified, individual GAG chains attached to the aggrecan core protein were clearly visualized. Physical evidence of two different densities of the CS-GAG brush regions was observed for the fetal epiphyseal and mature nasal aggrecan (Fig. 8). GAG spacing along the mature aggrecan of Fig. 8 was 72% greater than that of the fetal epiphyseal monomer. The measured spacing of 3.2 and 4.4 nm for fetal epiphyseal and mature nasal, respectively, correlates well with the predicted attachment of GAGs at the Ser–Gly residues based on the amino acid sequence of the core protein (Hering et al., 1997). The difference may be attributed to the number increase in shorter KS chains in the CS-GAG brush region in the mature aggrecan compared to the fetal aggrecan as demonstrated by the FACE compositional analyses (Fig. 1). KS content has been shown to increase with age (Bayliss and Ali, 1978). The distinguishing of individual CS chains (~25 kDa) from the shorter KS chains (~5–15 kDa) in this region was not possible due to similarity in size and location of the chains. However, the substitution of KS for CS may help to explain the decreased GAG spacing as measured from AFM images. Analysis of GAG composition and sulfation was done to differentiate the aggrecan populations, and to obtain biochemical structural information that could not be obtained through AFM.

The trace length measurements of the CS-GAG chains showed that L_c of fetal aggrecan was longer than that of mature aggrecan, and those values compared well with the hydrodynamic radius determined via chromatography. The resolution of the Superose 6 column is ± 0.4 K_{av} (~5 disaccharides ≈6 nm), and the resolution of the AFM at this level is less than a few nm. The difference between chromatography and AFM measurements may reflect inherent differences in the parameters being measured by those two techniques, as well as the slightly collapsed state of the GAG chains when moved from a fluid to an ambient 2D environment. Small sub-nm bend angles at the disaccharide level cannot be resolved in the AFM images. However, L_c as well as the extension and conformation of the GAG chains could be extracted from the AFM images. The average extension of the CS-GAG chains was ~78% for both fetal and mature populations (as compared to ~65% for the core protein), indicating that typically, monomers and GAG chains preferred an extended arrangement.

4.4. Aggrecan and GAG persistence length

Persistence length calculations from AFM images have been performed on linear biological polysaccharides such as mucins (Round et al., 2002), succinoglycan (Balnois et al., 2000), and xanthan (Camesano and Wilkinson, 2001). Complications arise in comparing the use of a WLC model for a simple polymer chain to that of the complex structure of aggrecan. Due to the close proximity of the charged GAG chains in a physiologic fluid environment, the GAGs as well as the core protein will take on a brush-like conformation. Charge repulsion and excluded volume play a role in creating this shape. However, a slight collapse of the structure may have occurred when moving from a fluid environment to an ambient environment. As described previously (Rivetti et al., 1996), the number of macromolecular conformations may be dramatically reduced by the constraining transition from three to two dimensions after physisorption from solution onto a surface. For weak intermolecular-surface interactions the macromolecules can rearrange and equilibrate on the surface as they would in a 2D solution, while for stronger interactions, the molecules are quickly fixed to the surface in a conformation that is close to a 2D mathematical projection of the 3D solution conformation onto the surface. For the first case (weak binding), the lowest energy conformation of the macromolecules existing in a 2D space are achieved and thus, meaningful structural information can be extracted from the 2D images (Rivetti et al., 1996). For the second case (strong binding), "kinetic trapping" of the molecules on the surface takes place and conformations are determined by the details of the approach to the surface (e.g.. diffusion processes) and the nature of the intermolecular surface forces (e.g., adsorption and solvent evaporation). In addition, the 2D conformation can be modified and biased by the lateral force exerted by the probe tip during imaging, which for tapping mode in air with capillary forces can be up to 9 nN for a tip radius of 10 nm (Shao et al., 1996).

The non-zero kurtosis for lower values of l suggest that the assumptions inherent to the WLC approach may not apply as well in this range of l for complex glycosylated molecules like aggrecan, whose contour trace length is not an order of magnitude longer than L_p. Nevertheless, the distributions of θ for aggrecan and GAGs were reasonably consistent with the distribution of θ predicted by the WLC model for larger l (Fig. 11C). We therefore used the WLC model to calculate an effective persistence length L_p and found that the fetal aggrecan was significantly stiffer ($L_p = 110$ nm) than the mature aggrecan ($L_p = 82$ nm). The shorter persistence length of the mature aggrecan is consistent with several other nanostructural measurements obtained from these images, since the increased CS-GAG spacing and

shorter chain lengths of the mature aggrecan would be expected to result in reduced stiffness, which is reflected in both the shorter persistence length and the shorter end-to-end length. CS-GAGs may individually satisfy the assumptions of the WLC model; however, the influence of inter- and intramolecular repulsion of chains through polyelectrolyte effects due to intramolecular electrostatic double layer repulsion, as well as excluded volume, which is amplified by close proximity of the chains is manifested in an increased effective L_p to an extended rigid-rod type conformation. Although we observed a higher mean stiffness for the fetal GAG, the difference in effective L_p was not statistically significant. It is important to note that conformation into a 2D state brings the CS-GAG chains closer in proximity to each other compared to a 3D state in which the CS chains are allowed to extend without constriction in a certain direction. This and excluded volume may lead to a slightly increased calculated L_p for both whole aggrecan as well as single CS chains. Further study is needed to verify that assumptions in the WLC model are valid for these molecules under the conditions of our experiments.

4.5. Comments on the relation of AFM experiments to native physiological conditions

From the appearance of the aggrecan monolayer in Fig. 5, we can estimate a corresponding 3D aggrecan density and compare with the known concentration of aggrecan in native cartilage (20–80 mg/ml). When modeled as 2D and flat, the thickness of aggrecan would be on the order of 1–10 nm based on GAG dimensions; thus, a compacted monolayer thickness of 1–10 nm would give an aggrecan concentration of 15–150 mg/ml, which brackets the physiological range. This calculation suggests that the GAG density pictured in Fig. 5 is likely to be on the order of that found in fully hydrated (3D) native cartilage. Alternatively, if we fix the positions of the core protein in Fig. 5 and assume that the fully hydrated thickness of each aggrecan would be approximately twice the length of the CS-GAG chain (i.e., $\sim$100 nm), the aggrecan density pictured in Fig. 5 would correspond to $\sim$1.5 mg/ml, about 40$\times$ less than physiological concentration. This suggests that the aggrecan core density pictured in Fig. 5 is likely to be far less than that in tissue when extrapolated to 3D. Even on this experimentally generated dense surface, flexibility and interdigitation are seen between the aggrecan molecules and in the CS-GAG region. It is expected that by scaling up the density 40$\times$ greater than this compact space will certainly lead to a significant amount of interdigitation and repulsive interaction between the aggrecan GAG chains. Moreover, with this high density of aggrecan at the tissue level, these nm-sized differences in aggrecan structure multiply quickly and can be translated into major differences in the compressive moduli of cartilage.

4.6. Conclusions

The fetal aggrecan was obtained from epiphyseal cartilage, which comes from the load-bearing region of an articulating joint. The mature aggrecan was obtained from nasal cartilage, which provides a static shape but is not subjected to repeated mechanical loading. While the basic structure of aggrecan from these two cartilaginous tissues is similar, there are clear differences which may be associated with tissue mechanical function. In confined compression, the equilibrium modulus of human articular cartilage was $\sim$600 kPa (Treppo et al., 2000) and that of human nasal cartilage was 233 kPa (Rotter et al., 2000). These data correlate nicely with the findings reported here that aggrecan from the load-bearing epiphyseal cartilage has a denser CS-GAG brush region, longer CS chains, and a greater calculated stiffness which might be expected when compared to the non-load-bearing nasal cartilage. Visualization of dense monolayers of these two aggrecan types gives important clues as to how neighboring aggrecan molecules may deform to accommodate each other under the highly compressed situations found in native cartilage.

Measurements on individual aggrecan molecules and constituent GAG chains were correlated to bulk measurements determined from standard biochemical techniques. In addition, the ability to measure single molecules in their near native state provides additional information on structure and conformation. Distinct differences between two aggrecan populations (e.g., mature nasal versus fetal epiphyseal) have been clearly observed and hence, it is clear that AFM studies of molecular constituents as a function of age, disease, and injury have great promise to yield new insights into for example, proteolytic degradation, and the molecular origins of cartilage dysfunction. Given the biochemical data confirming the presence of full-length aggrecan for both fetal and mature in conjunction with the measured dimensions of an overall shorter and a broader distribution of contour length of mature aggrecan core protein, it can be speculated that the increase in spacing between GAGs and decrease in GAG length results in a diminished repulsion between GAG chains, allowing the amino acid sequence of the protein core backbone to take on a lower energy state (i.e., from a strained linear shape to a relaxed coiled shape), thereby resulting in a shorter overall contour length. Decreased persistence length (i.e., stiffness) of the mature aggrecan may be a direct result of the reduced electrostatic repulsion in the CS-brush region.

AFM also has the potential to directly study the interaction between aggrecan and hyaluronan and the self-assembly process of the proteoglycan aggregate. Surfaces like this will allow for the measurement of intermolecular forces between a biomimetic surface such

as a CS-coated tip or an aggrecan-coated tip versus an aggrecan-coated surface. Such nanoscale information is critical to the understanding and prediction of cartilage intermolecular forces (e.g., electrostatic double layer, steric, etc.) and unique nanoscale deformation mechanisms (e.g. interdigitation versus compression) responsible for macroscopic biomechanical function (Dean et al., 2003).

Acknowledgments

Supported by the DuPont-MIT Alliance, NIH Grant AR45779, NIH Grant AR33236, Shriners Grant #8520 (JS), The Arthritis Foundation (AP), and a Whitaker Foundation Graduate Fellowship (LN).

References

Balnois, E., Stoll, S., Wilkinson, K.J., Buffle, J., Rinaudo, M., Milas, M., 2000. Conformation of succinoglycan as observed by atomic force microscopy. Macromolecules 33, 7440–7447.

Bayliss, M.T., Ali, S.Y., 1978. Age-related changes in the composition and structure of human articular-cartilage proteoglycans. Biochem. J. 176, 683–693.

Buckwalter, J., Rosenberg, L., Tang, L.-H., 1984. The effect of link protein on proteoglycan aggregate structure. J. Biol. Chem. 259, 5361–5363.

Buckwalter, J.A., Rosenberg, L.C., 1982. Electron microscopic studies of cartilage proteoglycans: direct evidence for the variable length of the chondroitin sulfate-rich region of proteoglycan subunit core protein. J. Biol. Chem. 257, 9830–9839.

Buckwalter, J.A., Rosenberg, L.C., 1983. Structural changes during development in bovine fetal epiphyseal cartilage. Coll. Rel. Res. 3, 489–504.

Buckwalter, J.A., Rosenberg, L.C., 1988. Electron microscopic studies of cartilage proteoglycans. Electron Microsc. Rev. 1, 87–112.

Buschmann, M.D., Grodzinsky, A.J., 1995. A molecular model of proteoglycan-associated electrostatic forces in cartilage mechanics. J. Biomech. Eng. 117 (2), 179–191.

Calabro, A., Midura, R.J., Wang, A., West, L.A., Plaas, A.H.K., Hascall, V.C., 2001. Fluorophore-assisted carbohydrate electrophoresis (FACE) of glycosaminoglycans. Osteoarthritis Cartilage 9, S16–S22.

Camesano, T.A., Wilkinson, K.J., 2001. Single molecule study of xanthan conformation using atomic force microscopy. Biomacromolecules 2, 1184–1191.

Cleland, R.L., 1977. Persistence length of hyaluronic acid: an estimate from small-angle X-ray scattering and intrinsic viscosity. Arch. Biochem. Biophys. 180, 57–68.

Cleland, R.L., Wang, J.L., 1970. Ionic polysaccharides. III. Dilute solution properties of hyaluronic acid fractions. Biopolymers 9, 799–810.

Cowman, M.K., Lin, M., Balazs, E.A., 1998. Tapping mode atomic force microscopy of hyaluronan: extended and intramolecularly interacting chains. Biophys. J. 75, 2030–2037.

Dean, D., Seog, J., Ortiz, C., Grodzinsky, A.J., 2003. A new molecular-level theoretical model for the electrostatic interactions between polyelectrolyte macromolecules using glycosaminoglycans as model system. Langmuir 19, 5526–5539.

Deutsch, A.J., Midura, R.J., Plaas, A.K., 1995. Structure of chondroitin sulfate on aggrecan isolated from bovine tibial and costochondral growth plates. J. Orthop. Res. 13, 230–239.

Diggle, P., Liang, K.-Y., Zeger, S.L., 1994. Analysis of Longitudinal Data. Clarendon Press, Oxford University Press, Oxford, New York. xi, 253pp.

Dudhia, J., Davidson, C.M., Wells, T.M., Vynios, D.H., Hardingham, T.E., Bayliss, M.T., 1996. Age-related changes in the content of the C-terminal region of aggrecan in human articular cartilage. Biochem. J. 313, 933–940.

Farndale, R.W., Buttle, D.J., Barrett, A.J., 1986. Improved quantitation and discrimination of sulphated glycosaminoglycans by use of dimethylmethylene blue. Biochim. Biophys. Acta 883, 173–177.

Flannery, C.R., Lark, M.W., Sandy, J.D., 1992. Identification of a stromelysin cleavage site within the interglobular domain of human aggrecan: evidence for proteolysis at this site in vivo in human articular cartilage. J. Biol. Chem. 267, 1008–1014.

Hascall, V.C., Sajdera, S.W., 1969. Proteinpolysaccharide complex from bovine nasal cartilage: the function of glycoprotein in the formation of aggregates. J. Biol. Chem. 224, 2384–2396.

Hascall, V.C., Sajdera, S.W., 1970. Physical properties and polydispersity of proteoglycan from bovine nasal cartilage. J. Struct. Biol. 245, 4920–4930.

Hering, T.M., Kollar, J., Huynh, T.D., 1997. Complete coding sequence of bovine aggrecan: comparative structural analysis. Arch. Biochem. Biophys. 345, 259–270.

Hunziker, P.R., Stolz, M., Aebi, U., 2002. Nanotechnology in medicine: moving from the bench to the bedside. Chimia 56, 520–526.

Jarchow, J., Fritz, J., Anselmetti, D., Calabro, A., Hascall, V.C., Gerosa, D., Berger, M.M., Busquets, X.-F., 2000. Supramolecular structure of a new family of circular proteoglycans mediating cell adhesion in sponges. J. Struct. Biol. 132, 95–105.

Jurvelin, J.S., Muller, D.J., Wong, M., Studer, D., Engel, A., Hunziker, E.B., 1996. Surface and subsurface morphology of bovine humeral articular cartilage as assessed by atomic force and transmission electron microscopy. J. Struct. Biol. 117, 45–54.

Kratky, O., Porod, G., 1949. Röntgenuntersuchung gelöster fadenmoleküle. Recl. Trav. Chim. Pays-Bas. 68, 1106.

Maroudas, A., 1979. In: Freeman, M.A.R. (Ed.), Physico-chemical Properties of Articular Cartilage in Adult Articular Cartilage. Pitman, England, pp. 215–290.

Mathews, M.B., Decker, L., 1977. Conformation of hyaluronate in neutral and alkaline solutions. Biochim. Biophys. Acta 498, 259–263.

Morgelin, M., Paulsson, M., Hardingham, T.E., Heinegard, D., Engel, J., 1988. Cartilage proteoglycans: assembly with hyaluronate and link protein studies by electron microscopy. Biochem. J. 253, 175–185.

Morgelin, M., Paulsson, M., Malmstrom, A., Heinegard, D., 1989. Shared and distinct features of interstitial proteoglycans from different bovine tissues revealed by electron microscopy. J. Biol. Chem. 264, 12080–12090.

Ng, L.J., Plaas, A.H.K., Grodzinsky, A.J., Ortiz, C., 2002. Structure, Conformation, and Self-Assembly of Cartilage Polyelectrolyte Macromolecules Studied via Atomic Force Microscopy, Polymer Preprints, vol, 224:351-POLY Part 2 The American Chemical Society (ACS), National Meeting, Division of Polymer Chemistry, Boston, MA.

Ng, L.J., Plaas, A.H.K., Ortiz, C., Grodzinsky, A., 2003a. AFM imaging of the conformation and interactions of aggrecan, hyaluronan, and their constituents, Trans. 49 Ortho. Res. Soc, 224, New Orleans, LA, USA.

Ng, L.J., Tai, K., Plaas, A.H.K., Grodzinsky, A.J., Ortiz, C., 2003b. Ultrastructure and Nanomechanics of Biological Tissues: Cartilage and Bone, The Annual Meeting of the American Chemical Society, Polymer Science and Engineering Division, Symposium on "Scanning Probe Microscopy of Polymers," New Orleans, LA, USA, Polymer Preprints (Full citation not available yet).

Paulsson, M., Morgelin, M., Wiedemann, H., Beardmore-Gray, N., Dunham, D., Hardingham, T., Heinegard, D., Timpl, R., Engel, J., 1987. Extended and globular protein domains in cartilage proteoglycans. Biochem. J. 245, 763–772.

Perkins, S.J., Miller, A., Hardingham, T.E., Muir, H., 1981. Physical properties of the hyaluronate binding region of proteoglycan from pig laryngeal cartilage: densitometric and small angle neutron scattering studies of carbohydrates and carbohydrate–protein macromolecules. J. Mol. Biol. 150, 69–95.

Plaas, A.H.K., West, L.A., Midura, R.J., 2001. Keratan sulfate disaccharide composition determined by FACE analysis of keratanase II and endo-beta-galactosidase digestion products. Glycobiology 11, 779–790.

Plaas, A.H.K., Wong-Palms, S., Roughley, P.J., Midura, R.J., Hascall, V.C., 1997. Chemical and immunological assay of the nonreducing terminal residues of chondroitin sulfate from human aggrecan. J. Biol. Chem. 272, 20603–20610.

Raspanti, M., Congiu, T., Guizzardi, S., 2001. Tapping-mode atomic force microscopy in fluid of hydrated extracellular matrix. Matrix Biol. 20, 601–604.

Rivetti, C., Guthold, M., Bustamante, C., 1996. Scanning force microscopy of DNA deposited onto mica: equilibration versus kinetic trapping studied by statistical polymer chain analysis. J. Mol. Biol. 264, 919–932.

Rosenberg, L., Hellmann, W., Kleinschmidt, A.K., 1970. Macromolecular models of proteinpolysaccharides from bovine nasal cartilage based on electron microscope studies. J. Biol. Chem. 245, 4123–4130.

Rotter, N., Tobias, G., Lebl, M., Roy, A.K., Hansen, M.C., Vacanti, C.A., Bonassar, L.J., 2000. Age-related changes in the composition and mechanical properties of human nasal cartilage. Arch. Biochem. Biophys. 403, 132–140.

Round, A.N., Berry, M., McMaster, T.J., Stoll, S., Gowers, D., Corfield, A.P., Miles, M.J., 2002. Heterogeneity and persistence length in human ocular mucins. Biophys. J. 83, 1661–1670.

Sandy, J.D., Verscharen, C., 2001. Analysis of aggrecan in human knee cartilage and synovial fluid indicates that aggrecanase (ADAMTS) activity is responsible for the catabolic turnover and loss of whole aggrecan whereas other protease activity is required for C-terminal processing in vivo. Biochem. J. 358, 615–626.

Seog, J., Dean, D., Plaas, A.H.K., Wong-Palms, S., Grodzinsky, A.J., Ortiz, C., 2002. Direct measurement of glycosaminoglycan intermolecular interactions via high-resolution force spectroscopy. Macromolecules 35, 5601–5615.

Shao, Z., Mou, J., Czajkowsky, D.M., Yang, J., Yuan, J.Y., 1996. Biological atomic force microscopy: what is achieved and what is needed. Adv. Phys. 45, 1–86.

Sheiko, S.S., 2000. Imaging of polymers using scanning force microscopy: from superstructures to individual molecules. Adv. Polym. Sci. 151, 62–174.

Sheiko, S.S., Moller, M., 2001. Visualization of macromolecules: a first step to manipulation and controlled response. Chem. Rev. 101, 4099–4123.

Tamayo, J., Garcia, R., 1996. Deformation, contact time, and phase contrast in tapping mode scanning force microscopy. Langmuir 12, 4430–4435.

Tanaka, K., 1978. Physiochemical properties of chondroitin sulfate: ion binding and secondary structure. J. Biochem. (Japan) 83, 647–653.

Todd, B.A., Rammohan, J., Eppell, S.J., 2003. Connecting nanoscale images of proteins with their genetic sequences. Biophys. J. 84, 3982–3991.

Treppo, S., Koepp, H., Quan, E.C., Cole, A.A., Kuettner, K.E., Grodzinsky, A.J., 2000. Comparison of biomechanical and biochemical properties of cartilage from human knee and ankle. J. Orthop. Res. 18, 739–748.

Yamamoto, S., Hitomi, J., Shigeno, M., Sawaguchi, S., Abe, H., Ushiki, T., 1997. Atomic force microscopic studies of isolated collagen fibrils of the bovine cornea and sclera. Arch. Histol. Cytol. 60, 371–378.